



Article

# Investigating the Hall-Petch Constants for As-Cast and Aged AZ61/CNTs Metal Matrix Composites and Their Role on Superposition Law Exponent

Aqeel Abbas and Song-Jeng Huang \*

Department of Mechanical Engineering, National Taiwan University of Science and Technology, No. 43, Section 4, Keelung Road, Taipei 10607, Taiwan; engr.aqeel14@gmail.com

\* Correspondence: [sgjghuang@mail.ntust.edu.tw](mailto:sgjghuang@mail.ntust.edu.tw)

**Abstract:** AZ61/carbon nanotubes (CNTs) (0, 0.1, 0.5, and 1 wt.%) composites were successfully fabricated by using the stir-casting method. Hall–Petch relationship and superposition of different strengthening mechanisms were analyzed for aged and as-cast AZ61/CNTs composites. Aged composites showed higher frictional stress (108.81 MPa) than that of as-cast (31.56 Mpa) composites when the grain size was fitted directly against the experimentally measured yield strength. In contrast, considering the superposition of all contributing strengthening mechanisms, the Hall–Petch constants contributed by only grain-size strengthening were found ( $\sigma_0 = 100.06$  Mpa and  $K_f = 0.3048$  Mpa  $m^{1/2}$ ) for as-cast and ( $\sigma_0 = 87.154$  Mpa and  $K_f = 0.3407$  Mpa  $m^{1/2}$ ) for aged composites when superposition law exponent is unity. The dislocation density for the as-cast composites was maximum ( $8.3239 \times 10^{13} m^{-2}$ ) in the case of the AZ61/0.5 wt.%CNT composite, and for aged composites, it increased with the increase in CNTs concentration and reached the maximum value ( $1.0518 \times 10^{14} m^{-2}$ ) in the case of the AZ61/1 wt.%CNT composite.

**Keywords:** AZ61/CNTs composites; superposition law; grain boundary; dislocation density; Hall–Petch constants



**Citation:** Abbas, A.; Huang, S.-J. Investigating the Hall-Petch Constants for As-Cast and Aged AZ61/CNTs Metal Matrix Composites and Their Role on Superposition Law Exponent. *J. Compos. Sci.* **2021**, *5*, 103. <https://doi.org/10.3390/jcs5040103>

Academic Editors:

Francesco Tornabene and Konda Gokuldoss Prashanth

Received: 27 February 2021

Accepted: 6 April 2021

Published: 9 April 2021

**Publisher's Note:** MDPI stays neutral with regard to jurisdictional claims in published maps and institutional affiliations.



**Copyright:** © 2021 by the authors. Licensee MDPI, Basel, Switzerland. This article is an open access article distributed under the terms and conditions of the Creative Commons Attribution (CC BY) license (<https://creativecommons.org/licenses/by/4.0/>).

## 1. Introduction

Magnesium alloys are the lightest structural materials with extensive applications in aerospace, automobiles, electronics, and mobiles due to their low density, absolute recyclability, high specific strength, and stiffness. Magnesium alloys possess low ductility, poor strength, and hard formability, which limit their widespread applications. Consequently, it is desired to take some effective measures to improve strength. One of the essential ways to improve the strength is contributing to the solid solution by using different reinforcements (carbon nanotubes (CNTs),  $Al_2O_3$ ,  $B_4C$ , Ti, and  $WS_2$ ), followed by various processes, like heat treatments for microstructure refinement [1–5]. It is a scorching topic in research to improve mechanical properties by the addition of reinforcement in magnesium alloy, followed by a process that causes the reduction in grain size [6].

The dislocation resistance offered by the distribution of strengthening obstacles leads to the formation of several metallurgical phenomena [7]. The flow resistance strength of the alloy is increased by enhancing the critical shear strength (CRS). To predict the CRS for polycrystalline materials, it is compulsory to investigate Taylor's factor. Depending on the composites' manufacturing route and composition, several multitudes of obstacles include grain size, Orowan, dispersoid, dislocation, and precipitates present in the microstructure [8]. The grain-boundary strengthening has gained significant importance in recent years. The materials' yield strength can be enhanced by refining the microstructure, using different processes, like severe plastic deformation, high-energy ball milling, elec-

trodeposition, and heat treatments [9–12]. The Hall–Petch relationship explains the reason for enhancement by grain-boundary strengthening:

$$\sigma_{gs} = \sigma_0 + K_f d^{-1/2} \quad (1)$$

where  $d$  is the average grain size. The  $\sigma_0$  is rationalized as frictional resistance to gliding dislocation.  $K_f$  is referred as the Hall–Petch constant and is a measure of grain boundary resistance to slip transfer. The Hall–Petch constants ( $\sigma_0$  and  $K_f$ ) are generally dependent on particle strengthening. The synthesized CNTs-reinforced AZ61 magnesium alloys have many defects (dislocations) and impurities. Other strengthening mechanisms at room temperature contribute to the overall strength of the composites. In this view, considering only experimentally measured yield strength values to evaluate the grain-boundary dislocation pile-up contribution in yield strength is not an appropriate method.

In the present study, the ageing effect was investigated on Hall–Petch (HP) constants ( $\sigma_0$  and  $K_f$ ) and their dependency on grain size. The true values of HP constants were extracted by isolating the grain-size contribution from other strengthening mechanisms for the appropriate value of the superposition law exponent.

## 2. Materials and Methods

AZ61 reinforced with multi-walled carbon nanotubes (CNTs) was produced by the stir-casting method [13]. The detailed manufacturing method and heat-treatment procedures are explained in our previously published paper [13]. The SEM (model JSM-6390LV) microstructure and XRD (Bruker D2 phaser) analysis were used to determine the grain size and strengthening mechanisms. The ASTM-E3 metallographic techniques were employed to investigate the microstructure. The experimental yield tensile strength was determined from materials testing systems (MTS-100), at the deformation rate of 0.5 mm/min. The origin pro software was used to plot the XRD and strengthening mechanism contribution. The average grain was measured by using ImageJ software.

## 3. Results and Discussion

### 3.1. Microstrain and Dislocation Density

The XRD results were used to quantify the microstrain and dislocation density [13]. The microstrain can be obtained by the by Williamson–Hall equation:

$$\beta \cos \theta = \frac{k\lambda}{L} + C\epsilon \sin \theta \quad (2)$$

where  $\beta$  is the full-width at half maximum (FWHM) of the diffraction peak,  $k$  is the Scherer constant (0.9),  $\lambda$  is the X-ray wavelength (1.5406 Å) for CuK $\alpha$  radiations,  $L$  is the crystallite size,  $\epsilon$  is microstrain, and  $\theta$  is the Bragg's angle. The  $\beta \cos \theta$  is plotted against  $C\epsilon \sin \theta$  by using XRD results. The approximate mean value of crystallite size obtained by intercept on the vertical axis and microstrain by the fitted line's slope. The Origin Pro software was used to analyze and extract the data from XRD results in integrated peaks. It can be observed from Figure 1 that the average microstrain distribution is maximum in as-cast 0.5 wt.%CNTs/AZ61 composites. For aged composites, microstrain distribution increases with the increase in CNTs concentration. The reasons for higher microstrain distribution are dislocation density, precipitation twinning effects, the smallness of crystallite size, microstresses, and phase heterogeneity [14]. The crystallite size of 0.5 wt.%CNTs/AZ61 was found to be the smallest. The smallness of crystallite size and heterogeneity is a significant stimulant in the development of microstrain in 0.5 wt.%CNTs/AZ61. The formation of a compressive microstrain indicates micro-plastic behavior in crystalline materials.

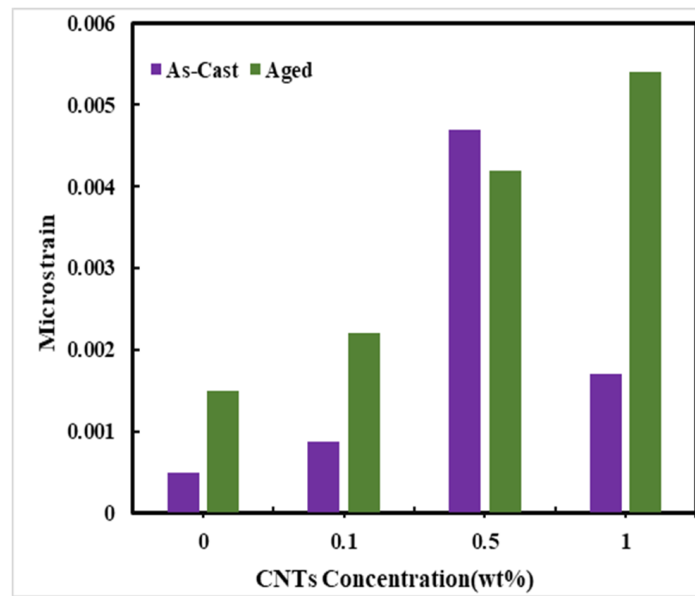


Figure 1. Microstrain distribution against carbon nanotubes (CNTs) concentration.

The dislocation densities of metal matrix composites (MMCs) were measured by using the relationship shown below:

$$\rho = \frac{3.4641\varepsilon}{Lb} \tag{3}$$

where  $\rho$  is the dislocation density,  $L$  is crystallite size,  $\varepsilon$  is microstrain, and  $b$  is burger vector ( $Mg \sim 0.325$  nm). It can be observed from Figure 2 that dislocation density increases with the increase in CNTs concentration in aged composites. It is clear from Equation (3) and Figure 2 that dislocation density is directly related to microstrain.

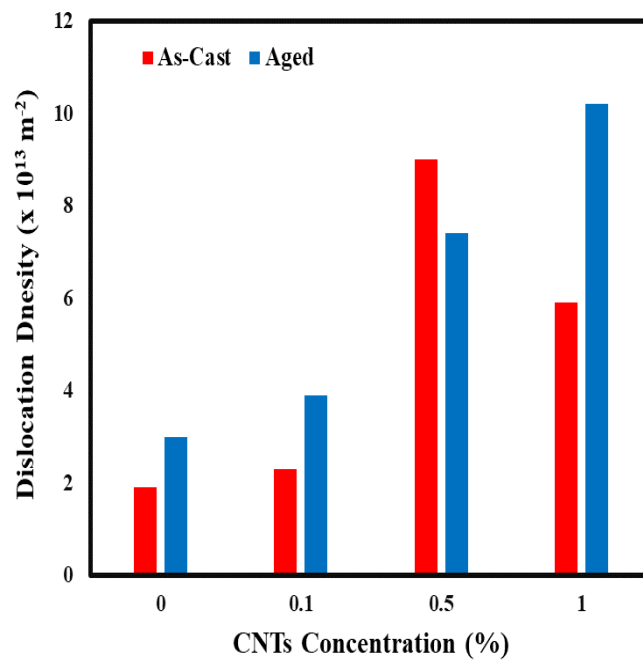


Figure 2. Dislocation density variation with CNTs concentration.

The influence of ageing heat treatment is significant in the dislocation density of magnesium-based metal matrix composites (MMCs) [15]. The considerable enhancement in dislocation density is due to the hindering effects of CNTs and the annihilation of phases

in aged composites. However, the increase in FWHM values due to heat treatment suggests the microstructural refinement and an increase in dislocation density [16]. The lower dislocation densities lead to more plastic flow in MMCs. The higher dislocation densities in aged composites are also attributed to grain size reduction and mismatch in the thermal expansion coefficient between AZ61 magnesium matrix and CNTs [17]. The following relation can predict the dislocation density due to the coefficient of thermal expansion:

$$\rho = \frac{B\varepsilon(V_m + V_r)}{bd(1 - (V_m + V_r))} \quad (4)$$

where B is the geometric constant,  $V_m$  and  $V_r$  are the volume fractions of the matrix (AZ61) and reinforcement (CNTs), b is the burger vector, and d is the grain diameter of the refined composite.

It can also be concluded that dislocation density is inversely proportional to grain size and residual stress [18]. The higher dislocation accelerates the global precipitation kinetics by promoting the nucleation in grain growth. The dislocations are produced in the vicinity of grain boundaries, owing to grain boundary strengthening mechanisms [19]. The main reason for ageing heat treatment was to produce the fine precipitates within the grains [20].

### 3.2. Microstructure Characterization

The SEM images of as-cast and aged AZ61/CNTs are presented in Figures 3 and 4, respectively. The average grain size of AZ61/CNTs is summarized in Figure 5. The addition of reinforcement and secondary processing contribute to yield strength by altering the microstructure. Several kinds of strengthening mechanism are undergone to determine the yield strength of the composite. The addition of CNTs has consumed several precipitates present in monolithic AZ61 (Figure 3). The set of contributing mechanisms is affected by the change in microstructure composition. The ageing heat treatment has further decreased the precipitation effects; grain boundaries are clearer, and pores are present at grain boundaries. The CNTs addition and ageing heat treatment have depleting effects on precipitation hardening, leading to increase in grain refinement strengthening (Figure 4). The volume, size, type, and distribution of precipitates have significant effects on precipitation hardening.

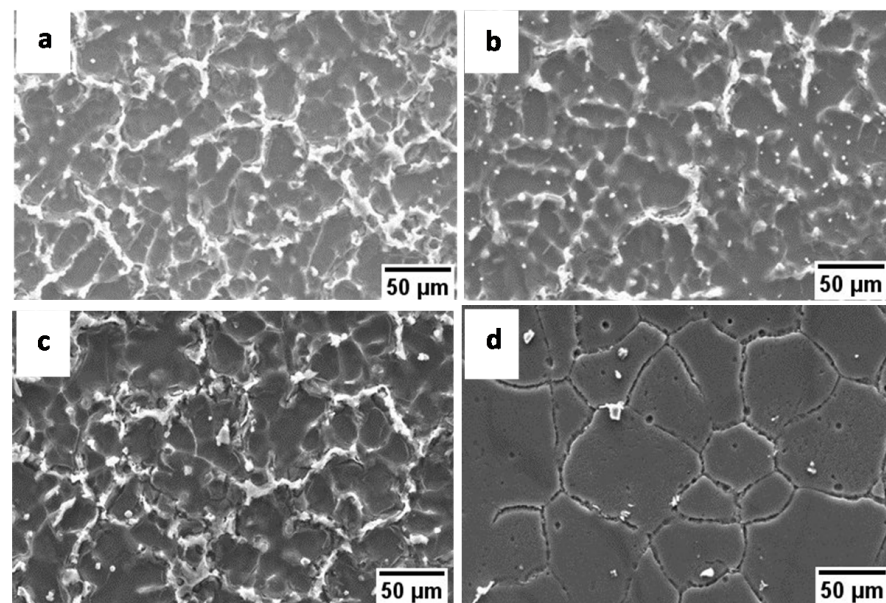


**Figure 3.** SEM images of as-cast AZ61 with CNTs: (a) 0 wt.%, (b) 0.1 wt.%, (c) 0.5 wt.%, and (d) and 1 wt.% [13].

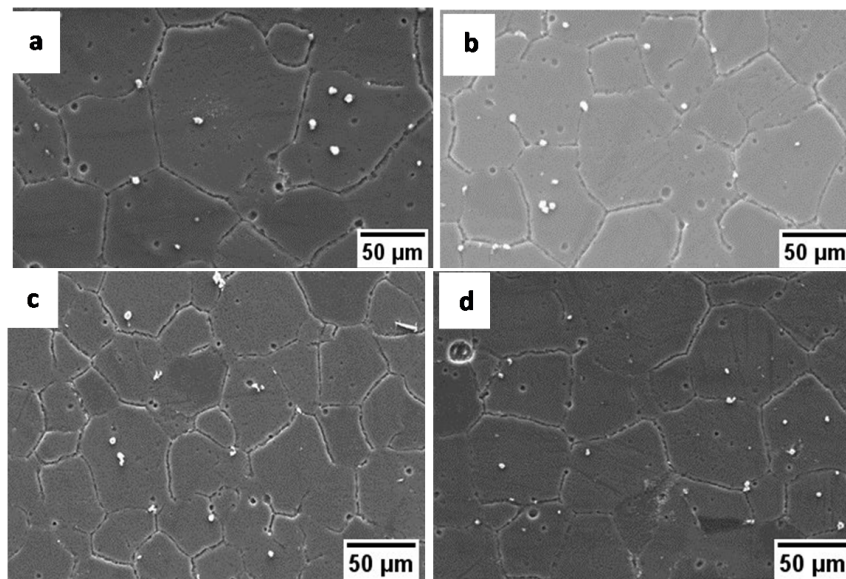


Figure 4. SEM images of aged AZ61 with CNTs: (a) 0 wt.%, (b) 0.1 wt.%, (c) 0.5 wt.%, and (d) 1 wt.% [13].

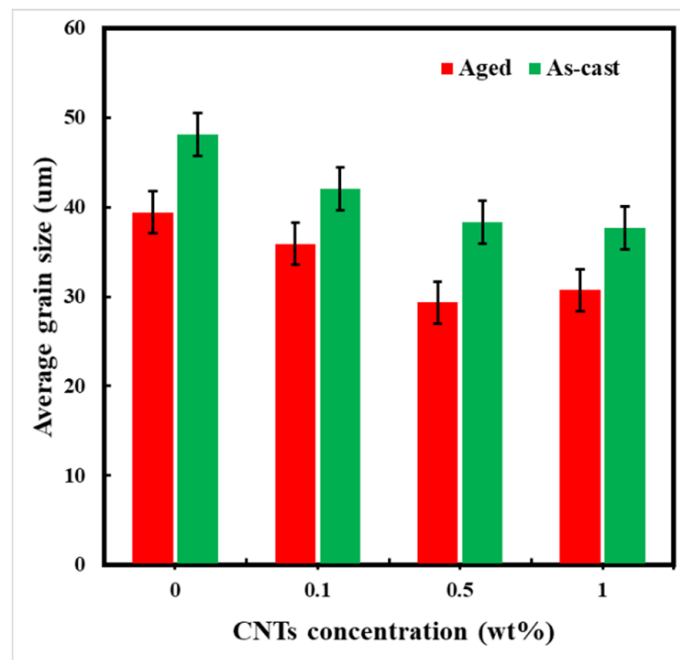


Figure 5. Average grain size AZ60/CNTs composites [13].

The precipitation parameters affect the Orowan strengthening contribution. The Orowan strengthening decreased with the increase of inter-precipitates spacing. The CNTs addition controls the vacancy to influence the interface phase spacing and interpret precipitation hardening. A large number of defects, such as dislocation density and deformation twins, are induced in the surface to form strain field in their vicinity, to generate stresses. Dislocation strengthening is a major strengthening mechanism that contributes in the strength of the alloy. The induced twinning defects also increase grain density and lead to solid solubility. Microalloying elements exist in the form of solid solution or in precipitates, and their role is distinctly clear. The load-transfer mechanism’s contribution is dependent on the aspect ratio. The quantitative fitting indicates the load transfer is not dominating mechanism to strengthen the composites. The increase in CNTs

concentration reduced the average grain size, and ageing heat treatment further decreased the grain size. The higher grain density leads to higher strength contribution by grain refinement. The coefficient of thermal expansion mismatch is also important parameter in microstructure refinement. The addition of CNTs developed the mismatch in thermal expansion, which also hinders the grain boundaries and breaks down the grains, making them smaller. The presence of pores at the grain boundaries leads to the depletion of some phases and improves grain refinement.

### 3.3. Hall–Petch Coefficient

Depending on the composition and manufacturing process, many obstacles contribute to strengthening the materials [21]. The most prominent obstacles include solid solution, dispersoids, grain boundaries, and dislocation density. The Hall–Petch relation is given by Equation (1) and is directly related to grain boundary strengthening. Moreover,  $\sigma_{(CTE)}$  is strength contributed by the coefficient of thermal expansion mismatch,  $\sigma_{(gs)}$  is strength due to grain refinement,  $\sigma_{(Ex)}$  is experimental yield strength, and  $\sigma_{(oth)}$  is yield strength contributed by all strengthening mechanisms other than grain size.

The grain-boundary strengthening has gained the most importance in ultrafine-grained and nanocrystalline materials for dramatic enhancement in yield strength of the composites [22]. The grain boundaries set up an obstacle to dislocation motion.

However, metallic composites have many obstacles that enhance strengthening and can be described by the Superposition law (Equation (5)):

$$\sigma_{YS} = \sigma_0 + \left( \sigma_{ss}^n + \sigma_{dis}^n + \sigma_{Orowan}^n + \sigma_{ppt}^n + \sigma_{gs}^n \right)^{\frac{1}{n}} \tag{5}$$

where  $\sigma_{ss}$  is solid solution strengthening,  $\sigma_{dis}$  dislocation hardening,  $\sigma_{ppt}$  precipitate strengthening, and  $n$  is superposition law exponent. The yield strength is not only dependent on grain boundary but also on other strengthening parameters. The superposition exponent is assumed to be 1 for the solid solution and dispersoid strengthening, as proposed by Ebeling and Ashby [23].

The yield strength of the composites was calculated experimentally during compression tests. The yield strength contributed by grain size was determined by subtracting the strength due to all other experimental yield strength obstacles. The grain size, experimental yield strength, and grain size contributed yield strength for all composites are given in Table 1. The experimentally determined yield strength is contributed by all obstacles mentioned in Equation (5). It is appropriate to determine yield strength contributed by grain size by using the following Equation (6).

$$\sigma_{gs} = \left( \sigma_{YS}^n - \sigma_{others}^n \right)^{\frac{1}{n}} \tag{6}$$

**Table 1.** Summary of grain size, experimental yield strength, contributing strengthens, and grain-size contributing strength.

Material	YS <sub>(Exp)</sub> (MPa)	Grain Size (µm)	σ <sub>(ss)</sub> (MPa)	σ <sub>(ppt)</sub> (MPa)	σ <sub>(CTE)</sub> (MPa)	σ <sub>(Oro)</sub> (MPa)	σ <sub>(gs)</sub> = ((σ <sub>Ex</sub> ) <sup>n</sup> - (σ <sub>oth</sub> ) <sup>n</sup> ) <sup>1/n</sup>		
							n = 0.5	n = 1	n = 1.5
0-AC	186	48	-	27	-	27	12.58	132	58.67
0.1-AC	216	42	19	29	25	29	9.195	114	50.67
0.5-AC	237	38	23	35	35	31	8.519	113	50.22
1-AC	316	37	31	41	47	39	10.413	158	70.22
0-Ag	195	39	7	34	-	31	10.958	123	54.67
0.1-Ag	266	35	19	43	29	36	10.080	139	61.78
0.5-Ag	325	30	23	51	35	44	11.317	172	76.45
1-Ag	369	28	31	63	47	57	10.276	171	76

The value of  $n$  is 0.5, 1, or 1.5. The grain size contributed yield strength with all three values of superposition exponent are presented in Table 2. The experimental yield strength and grain-size contributed yield strength are plotted against grain size in Figure 6. It can be revealed that Hall–Petch constants ( $\sigma_0$  and  $K_f$ ) values are different for as-cast, and aged composites under different values of “ $n$ ” are summarized in Table 2.

**Table 2.** Calculated values Hall–Petch constants ( $\sigma_0$  and  $K_f$ ) for different values of  $n$ .

Materials	$n = 0.5$		$n = 1$		$n = 1.5$		Experimental	
	K (Slope)	$\sigma$ (Intercept)	K (Slope)	$\sigma$ (Intercept)	K (Slope)	$\sigma$ (Intercept)	K (Slope)	$\sigma$ (Intercept)
As-Cast	0.0466	15.934	0.3407	87.154	0.1514	38.735	2.189	31.56
Aged	0.0028	11.121	0.3048	100.06	0.1355	44.469	1.0712	108.81

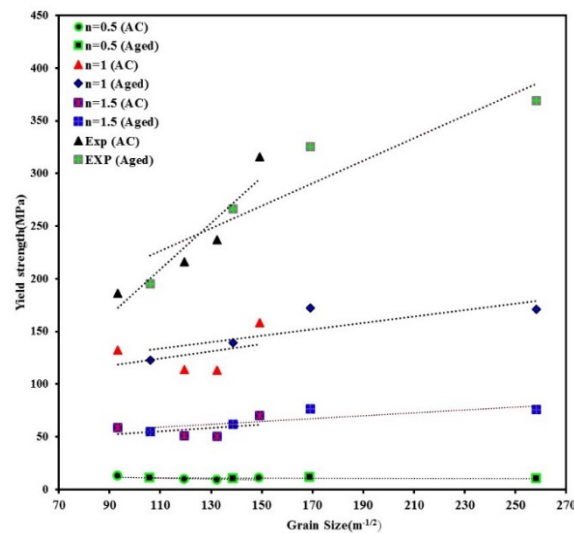


**Figure 6.** Hall–Petch relationship for different superposition law exponent values.

The maximum values for  $\sigma_0$  (108.81 MPa) and  $K_f$  (1.0712 MPa m<sup>1/2</sup>) were observed for aged composites when experimental yield strength was plotted against the grain size, as it relates that the yield strength is monotonous due to the grain boundary neglecting all other strengthening mechanisms. The lowest values for  $K_f$  (0.0028 m<sup>1/2</sup>) was observed for aged composites when exponent  $n = 0.5$ . The value of the superposition law exponent is of critical importance to determine  $\sigma_0$  and  $K_f$  for any composite. The minimum value of  $K_f$  was used to calculate the contributed grain-size strength, using Equation (1), and values were put into Equation (5) to estimate the yield strength. This is more due to the super-positioning of other strengthening contributions stemming from solute atoms, but, more importantly, from dispersoid and precipitate strengthening.

The strengthening effect of grain boundaries decreases with increasing CNTs contents in as-cast and aged composites for having higher stacking fault energy in CNTs [5]. The lower experimental values of ( $\sigma_0$ ) indicate higher plastic deformation during processing. The frictional strength was maximum ( $\sigma_0 = 87.154$  MPa) for as-cast composites when the superposition law exponent is unity.

The Hall–Petch mechanism proposed that grain boundaries enhance the strength by the pile-up of dislocation motion [24]. The yielding occurs when stress is large enough to propagate the slip/dislocation from one grain to another. The higher the frictional strength, the more stress is required to generate the dislocation, leading to enhanced yield strength. Implementing the Hall–Petch relation in the analysis of flow stress and friction stress of deformed materials is quite complex when boundaries of different characteristics having different resistance to dislocation subdivide the structure [22]. It has been suggested that

boundary strengthening is independent of the mode of formation by which crystalline alloy has been manufactured [25]. Stress occurs when dislocation piles up and reaches a critical value, which is necessary to nucleate dislocation across the grain boundary.

The grain boundaries subdividing the microstructure are divided into incidental grain boundary and geometric necessary grain boundaries [26]. The incidental grain boundaries are formed by trapping the glide dislocations, and geometric grain boundaries are produced by misorientation of induced lattice rotations [27]. There is a critical angle in dislocation boundaries below which grain boundary resistance increases with the increase in misorientation angle and below which dislocation boundary and high angle boundary show the same resistance. High-resolution electron microscopy is required to characterize the grain boundary structural parameters and analyze the strengthening mechanisms. Finally, to address the strength–structural phenomena, the frictional strength is dependent on grain-boundary characteristics.

The dependency of HP constants on superposition law exponent is significant from the above Figure 6, and it is adjustable to fit the experimental data points. The Pythagorean superposition exponent with  $n = 1$  is assumed to be best for obstacles having similar strength and obstacles having different strengths; superposition law exponent is close to unity. The approach is suitable for alloy systems which are strengthened by several strengthening mechanisms.

#### 4. Conclusions

An AZ61 magnesium alloy reinforced with CNTs was successfully fabricated by using the stir-casting method, followed by ageing heat treatments. The microstrain and dislocation density were found to be maximum for as-cast AZ61/0.5 wt.%CNTs and aged composites; they increased with the increase in CNTs contents and reached (0.00527) and ( $1.0518 \times 10^{14} \text{ m}^{-2}$ ), respectively, for 1 wt.%CNTs/AZ61. Hall–Petch analysis of experimental strength of composites resulted in higher frictional stress (108.81 MPa) and  $K_f$  (1.0712 MPa  $\text{m}^{1/2}$ ) for aged composites than those of as-cast composites. The maximum Hall–Petch constants ( $\sigma_0$  and  $K_f$ ) were observed for both as-cast and aged composites with linear superposition ( $n = 1$ ) of all contributing strengthening mechanisms. The true Hall–Petch constants are evaluated only when other contributing strengtheners are subtracted from the experimental yield strength in an inappropriate manner.

**Author Contributions:** A.A.: Methodology, Investigations, Writing draft; S.-J.H.: Conceptualization, Review and editing, Resources. All authors have read and agreed to the published version of the manuscript.

**Funding:** No funding was received from outside to conduct this research.

**Institutional Review Board Statement:** No ethical approval required.

**Informed Consent Statement:** Not applicable.

**Data Availability Statement:** There is no data available.

**Conflicts of Interest:** It is declared that we have no conflict of interest with any author or institute for this manuscript.

#### References

1. Raj, R.; Thakur, D.G. Qualitative and quantitative assessment of microstructure in Al-B4C metal matrix composite processed by modified stir casting technique. *Arch. Civ. Mech. Eng.* **2016**, *16*, 949–960. [CrossRef]
2. Habibnejad-Korayem, M.; Mahmudi, R.; Poole, W.J. Enhanced properties of Mg-based nano-composites reinforced with Al<sub>2</sub>O<sub>3</sub> nano-particles. *Mater. Sci. Eng. A* **2009**, *519*, 198–203. [CrossRef]
3. Huang, S.-J.; Abbas, A. Effects of tungsten disulfide on microstructure and mechanical properties of AZ91 magnesium alloy manufactured by stir casting. *J. Alloys Compd.* **2019**, *817*, 153321. [CrossRef]
4. Abbas, A.; Huang, S.-J. Qualitative and Quantitative Investigation of As-Cast and Aged CNT/AZ31 Metal Matrix Composites. *JOM* **2020**, *72*, 1–11. [CrossRef]

5. Abbas, A.; Huang, S.J.; Ballóková, B.; Sülleiová, K. Tribological effects of carbon nanotubes on magnesium alloy AZ31 and analyzing aging effects on CNTs/AZ31 composites fabricated by stir casting process. *Tribol. Int.* **2020**, *142*, 105982. [[CrossRef](#)]
6. Kumar, D.; Thakur, L. Recent Studies on the Fabrication of Magnesium Based Metal Matrix Nano-Composites by Using Ultrasonic Stir Casting Technique—A Review. *Mater. Sci. Forum* **2019**, *969*, 889–894. [[CrossRef](#)]
7. Thangaraju, S.; Heilmaier, M.; Murty, B.S.; Vadlamani, S.S. On the estimation of true Hall-Petch constants and their role on the superposition law exponent in Al alloys. *Adv. Eng. Mater.* **2012**, *14*, 892–897. [[CrossRef](#)]
8. Wang, X.; Hu, X.; Liu, W.; Du, J.; Wu, K.; Huang, Y.; Zheng, M. Ageing behavior of as-cast SiCp/AZ91 Mg matrix composites. *Mater. Sci. Eng. A* **2017**, *682*, 491–500. [[CrossRef](#)]
9. Abbas, A.; Huang, S.-J. Investigation of severe plastic deformation effects on microstructure and mechanical properties of WS<sub>2</sub>/AZ91 magnesium metal matrix composites. *Mater. Sci. Eng. A* **2020**, *780*, 139211. [[CrossRef](#)]
10. Abbas, A.; Huang, S.-J. ECAP effects on microstructure and mechanical behavior of annealed WS<sub>2</sub>/AZ91 metal matrix composite. *J. Alloys Compd.* **2020**, *835*, 155466. [[CrossRef](#)]
11. Huang, S.-J.; Rajagopal, V.; Chen, Y.L.; Chiu, Y.-H. Improving the hydrogenation properties of AZ31-Mg alloys with different carbonaceous additives by high energy ball milling (HEBM) and equal channel angular pressing (ECAP). *Int. J. Hydrogen Energy* **2019**, *45*, 22291–22301. [[CrossRef](#)]
12. Huang, S.-J.; Rajagopal, V.; Ali, A.N. Influence of the ECAP and HEBM processes and the addition of Ni catalyst on the hydrogen storage properties of AZ31-x Ni (x = 0, 2, 4) alloy. *Int. J. Hydrogen Energy* **2019**, *44*, 1047–1058. [[CrossRef](#)]
13. Huang, S.J.; Abbas, A.; Ballóková, B. Effect of CNT on microstructure, dry sliding wear and compressive mechanical properties of AZ61 magnesium alloy. *J. Mater. Res. Technol.* **2019**, *8*, 4273–4286. [[CrossRef](#)]
14. Huang, S.-J.; Ali, A.N. Effects of heat treatment on the microstructure and microplastic deformation behavior of SiC particles reinforced AZ61 magnesium metal matrix composite. *Mater. Sci. Eng. A* **2018**, *711*, 670–682. [[CrossRef](#)]
15. Liao, H.; Chen, J.; Peng, L.; Han, J.; Yi, H.; Zheng, F.; Wu, Y.; Ding, W. Fabrication and characterization of magnesium matrix composite processed by combination of friction stir processing and high-energy ball milling. *Mater. Sci. Eng. A* **2017**, *683*, 207–214. [[CrossRef](#)]
16. Máthis, K.; Farkas, G.; Garcés, G.; Gubicza, J. Evolution of dislocation density during compression of a Mg-Zn-Y alloy with long period stacking ordered structure. *Mater. Lett.* **2017**, *190*, 86–89. [[CrossRef](#)]
17. Ardeljan, M.; Beyerlein, I.J.; Knezevic, M. Mechanical response, twinning, and texture evolution of WE43 magnesium-rare earth alloy as a function of strain rate: Experiments and multi-level crystal plasticity modeling. *Int. J. Plast.* **2017**, *99*, 81–101. [[CrossRef](#)]
18. Pugazhenth, A.; Dinaharan, I.; Kanagaraj, G.; Selvam, J.D.R. Predicting the effect of machining parameters on turning characteristics of AA7075/TiB<sub>2</sub> in situ aluminum matrix composites using empirical relationships. *J. Braz. Soc. Mech. Sci. Eng.* **2018**, *40*, 555. [[CrossRef](#)]
19. Wu, C.; Shi, R.; Luo, G.; Zhang, J.; Shen, Q.; Gan, Z.; Liu, J.; Zhang, L. Influence of particulate B<sub>4</sub>C with high weight fraction on microstructure and mechanical behavior of an Al-based metal matrix composite. *J. Alloys Compd.* **2019**, *789*, 825–833. [[CrossRef](#)]
20. Otto, F.; Dlouhý, A.; Somsen, C.; Bei, H.; Eggeler, G.; George, E.P. The influences of temperature and microstructure on the tensile properties of a CoCrFeMnNi high-entropy alloy. *Acta Mater.* **2013**, *61*, 5743–5755. [[CrossRef](#)]
21. Gwalani, B.; Soni, V.; Lee, M.; Mantri, S.; Ren, Y.; Banerjee, R. Optimizing the coupled effects of Hall-Petch and precipitation strengthening in a Al<sub>0.3</sub>CoCrFeNi high entropy alloy. *Mater. Des.* **2017**, *121*, 254–260. [[CrossRef](#)]
22. Kato, M. Hall-Petch relationship and dislocation model for deformation of ultrafine-grained and nanocrystalline metals. *Mater. Trans.* **2014**, *55*, 19–24. [[CrossRef](#)]
23. Ashby, M. Work hardening of dispersion-hardened crystals. *Philos. Mag.* **1966**, *14*, 1157–1178. [[CrossRef](#)]
24. El-Tahawy, M.; Máthis, K.; Garcés, G.; Matsumoto, T.; Yamasaki, M.; Kawamura, Y.; Gubicza, J. Type and density of dislocations in a plastically deformed long-period stacking ordered magnesium alloy. *J. Alloys Compd.* **2019**, *771*, 629–635. [[CrossRef](#)]
25. Tian, C.; Li, X.; Li, H.; Guo, G.; Wang, L.; Rong, Y. The effect of porosity on the mechanical property of metal-bonded diamond grinding wheel fabricated by selective laser melting (SLM). *Mater. Sci. Eng. A* **2019**, *743*, 697–706. [[CrossRef](#)]
26. Okamoto, N.L.; Fujimoto, S.; Kambara, Y.; Kawamura, M.; Chen, Z.M.; Matsunoshita, H.; Tanaka, K.; Inui, H.; George, E.P. Effects of annealing on hardness, yield strength and dislocation structure in single crystals of the equiatomic Cr-Mn-Fe-Co-Ni high entropy alloy. *Sci. Rep.* **2016**, *6*, 35863. [[CrossRef](#)]
27. Wu, D.; Zhang, J.; Huang, J.; Bei, H.; Nieh, T.-G. Grain-boundary strengthening in nanocrystalline chromium and the Hall-Petch coefficient of body-centered cubic metals. *Scr. Mater.* **2013**, *68*, 118–121. [[CrossRef](#)]